Available online at www.sciencedirect.com
ScienceDirect
Organic Electronics 8 (2007) 136–147
Organic Electronics
www.elsevier.com/locate/orgel

Surface plasmon–polariton mediated emission of light from top-emitting organic light-emitting diode type structures

S. Wedge [a,*], A. Giannattasio [b], W.L. Barnes [a]

[a] Thin Films Photonics Group, School of Physics, Stocker Road, University of Exeter, Exeter EX4 4QL, UK
[b] Department of Materials, University of Oxford, Parks Road, Oxford OX1 3PH, UK

Received 6 February 2006; received in revised form 4 July 2006; accepted 7 July 2006
Available online 10 August 2006

Abstract

Surface plasmon–polariton (SPP) modes may act as significant loss channels in organic light-emitting diode devices. We present experimental data illustrating that by the introduction of an appropriately scaled microstructure into a device, some of this lost power may be recovered as light. It is shown that in order to maximize this SPP-mediated light emission in a top-emitting light-emitting diode (TOLED) the plasmon modes associated with the two metal surfaces of the cathode must be coupled together. Data from grating-coupled and index-coupled SPP schemes are presented, and we show that photoluminescence emission from a structure containing a microstructured thin metal film that supports coupled SPPs is at least 50 times more effective than a similar planar structure. Experimental data is also presented from a structure containing a thin metal film whose profile contains a wavelength scale microstructure on a single interface. These data suggest that such a device geometry has the potential to increase the efficiency of top-emitting organic light-emitting devices.

PACS: 85.60.Jb; 72.80.Le

Keywords: Surface plasmons; Organic light-emitting diodes (OLEDs); Microstructure

1. Introduction

Since it was first demonstrated that organic materials could be used to make organic light-emitting diodes (OLEDs) much work has concentrated on improving the efficiency of these devices. To this end, three main classes of organic materials have been considered for OLED fabrication; conjugated polymers, small molecules and conjugated dendrimers.

The first polymer device utilized poly(*p*-phenylene vinylene) as an emissive material and upon charge injection the resulting electroluminescence (EL) was emitted through a transparent substrate [1]. Subsequent polymer devices have implemented a number of schemes to address both the internal and external efficiency of the device. Methods of increasing internal efficiency have include the use of electron transport layers [2] to aid charge injection and phosphorescent dyes [3] to obtain light

* Corresponding author. Tel.: +44 1392 264157; fax: +44 1392 264111.
E-mail address: s.wedge@exeter.ac.uk (S. Wedge).

1566-1199/$ - see front matter
doi:10.1016/j.orgel.2006.07.003

from otherwise non-radiative triplet states. More recently increases in the external or optical efficiency of polymer devices have been sought by the use of periodic microstructure to scatter waveguided [4] and surface plasmon–polariton (SPP) modes [5] to light.

Initial studies into the use of organic small molecules as light-emitting layers employed the material tris(8-hydroxyquinoline)aluminium (Alq_3) [6]. As with polymer based devices improvements in device efficiency of small molecule OLEDs were sought. Approaches to increase device efficiency have included the addition of low work function materials to the cathode [7], oxygen plasma treatment of the anode [8] and again the use of microstructure to recover power lost to non-radiative modes [5,9]. Small molecule based OLEDs have also been considered where emission takes place through an optically thin metallic cathode [10]. Such top-emitting OLED (TOLED) devices have the capacity to be constructed on opaque silicon substrates. These TOLED devices have two advantages over substrate emitting OLEDs. Firstly, the use of a silicon substrate allows the integration of switching elements into this layer. Secondly, in a substrate emitting OLED between 50% and 80% of the light emission may be waveguided in the organic, anode and substrate layers [11] and the use of an opaque substrate may reduce these loses. As with substrate emitters efficiency improvements have been sought via the use of charge injection layers [12,13], tuning of the thickness of the electrodes [14] and the inclusion of highly reflective anodes [15].

The latest class of materials considered for OLED applications are conjugated dendrimers [16]. Emission of light from dendrimer materials occurs via phosphorescent, as opposed to fluorescence from both polymer and small molecule emitters and thus this class of material has the potential of producing highly efficient devices [17].

Above, it was noted that power dissipated to SPP modes supported by an OLED structure might be recovered as light by the introduction into the structure of a wavelength scale periodic microstructure. Due to the constructional geometry of OLEDs, where an emissive layer is bounded by metallic electrodes the existence of SPP modes is unavoidable. It has been demonstrated that power from the emitter may be lost to SPP modes associated with both the cathode/organic and anode/organic interfaces [18]. In a planar system SPP modes are non-radiative [19] and thus SPP modes may act to limit the efficiency of an OLED device. The power dissipated to SPP modes supported at metal/dielectric interfaces within an OLED depends greatly upon the class of emitter used [20]. This variation in dissipated power is primarily because of the orientation of the dipole moment of the different types of emissive material. For materials where the dipole moment may sample all directions in space on a time scale faster than the excited state lifetime, and are thus effectively isotropic, power is seen to be strongly coupled to SPP modes [21]. This is true of both small molecule and dendrimer emitters. In contrast, the dipole moment of conjugated polymers lie predominantly in the plane of the layers [22] and are therefore less strongly coupled to by SPP modes than either small molecule or dendrimer emitters [20].

The utilization of SPP modes as means to transmit light through thin metal films has been demonstrated in a number of studies [23,24]. In the context of TOLEDs the use of SPPs to augment the emission of light is particularly attractive. Moreover, recently it has been shown that the non-radiative decay of excitons within an emissive layer via coupling to SPP modes supported by TOLEDs may provide a significant loss channel, thus restricting device efficiency [18]. However, the use of SPP modes as a means of mediating light emission from TOLED devices remains relatively little explored. For this reason we examine here a number of schemes in which SPP modes can be used to transport energy across a metal film (cathode). These SPP modes are then scattered to light, from a wavelength scale microstructure. The application of such a device geometry may be of interest commercially and offers some unexpected challenges in understanding the physics involved.

2. Theory

SPPs are trapped surface modes that occur at the interface between a metal and a dielectric and have electromagnetic fields that decay exponentially into both the surrounding media [19]. On a planar surface SPPs are non-radiative in nature, this is due to the wavevector (momentum) of the SPP along the surface, $\boldsymbol{k}_{SPP}$, being greater than that of a photon ($\boldsymbol{k}_0$) in free space of the same frequency. Therefore in a device such as an OLED, in which a metallic cathode is bounded by a dielectric emissive layer, power that is coupled to SPPs is dissipated as heat and therefore lost.

The dispersion of the SPP mode for a simple metal/dielectric interface may be found by solving Maxwell's equations [19] and is given by

$$\boldsymbol{k}_{\mathrm{SPP}} = \boldsymbol{k}_0 \sqrt{\frac{\varepsilon_{\mathrm{d}}\varepsilon_{\mathrm{m}}}{\varepsilon_{\mathrm{d}} + \varepsilon_{\mathrm{m}}}}, \tag{1}$$

where ε_{d} and ε_{m} are the frequency-dependent relative permittivities of the dielectric material and metal, respectively. The non-radiative nature of the SPP may be overcome by the introduction into a device of a wavelength scale periodic microstructure (pitch λ_{g}) [23]. Such a microstructure may act to reduce/augment the momentum (wavevector) of the SPP mode, thus allowing the SPP to Bragg scatter to light according to the relation,

$$\boldsymbol{k}_{\mathrm{SPP}} \pm n\boldsymbol{k}_{\mathrm{g}} = \boldsymbol{k}_0 \sin\theta, \tag{2}$$

where $\boldsymbol{k}_{\mathrm{g}}$ is the grating wavevector ($|\boldsymbol{k}_{\mathrm{g}}| = 2\pi/\lambda_{\mathrm{g}}$), $\boldsymbol{k}_0 \sin\theta$ is in-plane wavevector of the radiated light, θ being the polar angle of the emitted light (see Fig. 2(b)) and n is an integer that defines the order of the scattering process. Here in-plane is the component of the wavevector in the plane of incidence and parallel to the layers of the structure. However, as will be shown below, the recovery of energy dissipated to SPP modes is more complex than the simple scattering process described by Eq. (2).

Emission from a TOLED takes place through a metallic cathode that is often of order 50 nm thick. This thickness is comparable with the decay length of the optical field into the metal so that excitons within the organic emissive material may couple to SPP modes supported at both the metal/organic medium and metal/air interfaces. However, the field of the organic emitter is exponentially attenuated on crossing the metal so that significantly more power is coupled to the SPP supported at the metal/organic interface than to the SPP associated with the metal/air interface [25]. This disparity of coupling strength between SPP supported on either side of a thin metal film is illustrated in Fig. 1 where the emitter has been modelled as an electric dipole at a distance of 20 nm from a 30 nm thick silver film [25]. From Fig. 1 it may be seen that the power dissipated by the emitter to the metal/organic SPP is approximately two orders of magnitude greater than that dissipated to the metal/air SPP. Although the coupling strength between the emitter and the metal/air SPP is relatively weak we will see that the existence of this mode may allow the transfer of energy from the metal/organic interface across the metal. This transfer of energy may be facilitated by coupling together the modes on either side of the metal by means of either grating-coupled or index-coupled SPPs. Here grating-coupling is the matching of the wavevectors of the SPP modes associated with each interface of a thin metal film via a periodic microstructure. Index-coupling is the matching of the SPP wavevectors by matching of the relative permittivities of the two media bounding a thin metal film.

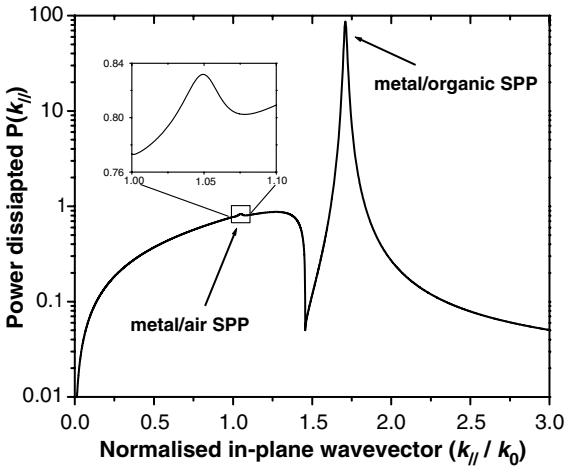

Fig. 1. Calculated power dissipation spectrum on a logarithmic scale for an emitter located in the light-emitting media at a distance of 20 nm from the surface of a 30 nm thick metal film. The large peak at a normalised in-plane wavevector of ~1.7 indicates power being lost to the metal/organic SPP, the inset is an expanded plot (linear scale) of the feature associated with the metal/air SPP.

If a metal is thin enough, of order tens of nanometres, the SPP fields associated with each interface of the metal may span the metal and overlap. Usually the metal film is bounded on either side by media with differing dielectric constants (refractive indices), i.e. an organic emitter and air, so that each of these SPP modes will have different in-plane wavevectors for a given frequency. The two SPP modes will therefore not be able to couple together. In order to couple these modes together, thus enabling energy to be transported across the metal some means must be sought to match the wavevectors of the two modes.

2.1. Grating-coupled SPPs

One method of coupling the SPP modes associated with each side of a thin metal film is SPP grating-coupling [24,26,27]. By adding an appropriately scaled periodic microstructure to the metal the wavevectors of the metal/organic SPP ($\boldsymbol{k}_{\mathrm{SPPorg}}$)

and the metal/air SPP (k_{SPPair}) may be matched when the following condition is satisfied.

$$\pm k_{SPPair} = \pm k_{SPPorg} \pm k_g \quad (3)$$

The metal/air SPP may subsequently be coupled to light, again via the microstructure by satisfying Eq. (2).

2.2. Index-coupled SPPs

Above it was noted that SPPs supported by a metal film bounded by differing refractive indices have different wavevectors. However, if the refractive indices of both bounding media are the same then the two SPP modes are degenerate and may therefore be coupled together [28]. The SPP modes supported by such a system will be coupled across all frequencies and energy may be transferred across the metal film without the need for the addition of a scattering surface. However, a microstructure is required in order to subsequently couple this plasmon energy to light. Below we explore the use of grating-coupled and index-coupled SPPs as a means of recovering energy lost to SPP modes.

3. Sample fabrication

To investigate the emission of light through a thin metal film mediated by SPP modes a number of different samples were constructed and are shown schematically in Fig. 2. Since we were interested here only in the underlying physics of the coupling of the SPP modes to light, it was sufficient to measure the SPP-mediated photoluminescence (PL) emission from an emissive layer through a thin metal film from each of these structures.

The first of these structures (Fig. 2(a)) was a planar control sample and consisted of a 60 nm thick emissive Alq_3 film deposited by thermal evaporation. The Alq_3 layer was subsequently coated with a thermally evaporated silver film (thickness 55 ± 2 nm) again by thermal evaporation under vacuum ($\sim 10^{-7}$ Torr). This structure was used as a reference sample.

The second structure (Fig. 2(b)) was used to investigate the use of a wavelength scale periodic microstructure to scatter SPP modes to light. This sample was similar in construction to the planar control structure (Fig. 2(a)) containing a 60 nm evaporated Alq_3 emissive layer and was coated with a metal film of thickness 55 ± 2 nm. However, the Ag film differed from that used in the above sample

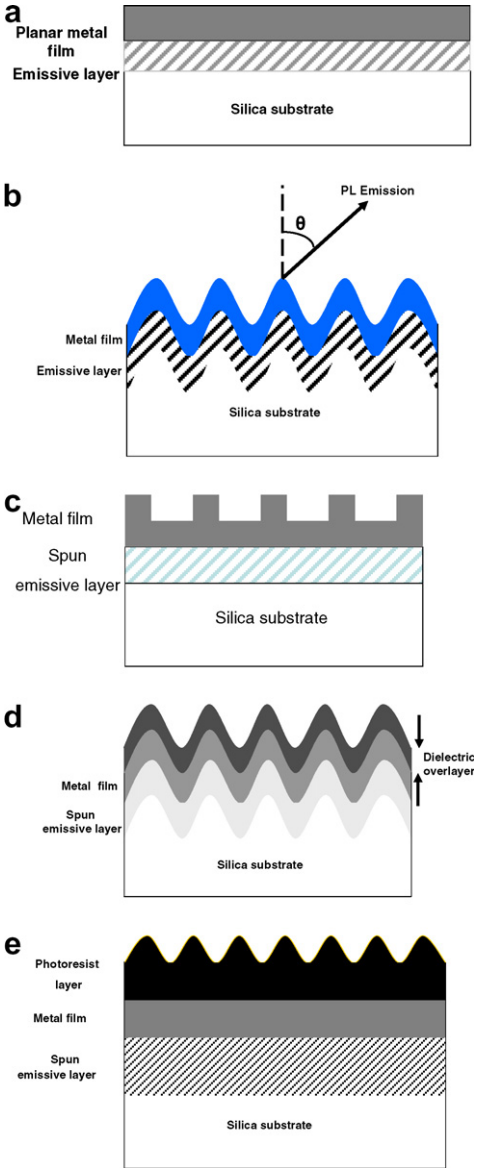

Fig. 2. Schematic representations of the experimental structures used in this study. (a) A 60 nm thick evaporated Alq_3 layer coated with a ~55 nm thick planar silver film. (b) An ~60 nm thick evaporated Alq_3 layer coated with a microstructured ($\lambda_g = 338$ nm) 55 nm thick silver film. (c) A 160 nm thick spun Alq_3 layer coated with a ~50 nm thick silver film where only the metal/air interface has been textured ($\lambda_g = 400$ nm). (d) An ~43 nm thick microstructured ($\lambda_g = 338$ nm) silver film bounded on one side by a 160 nm thick spun Alq_3 film and on the other by a dielectric overlayer (22-tric). (e) An ~55 nm thick planar silver film bounded on one side by a 160 nm spun Alq_3 layer and on the other by an ~100 nm thick microstructured ($\lambda_g = 485$ nm) photoresist overlayer.

in one important respect. The metal film included a wavelength scale microstructure ($\lambda_g = 338 \pm 1$ nm). This microstructure was produced by spin coating

the silica substrate with a ~300 nm thick photoresist (PR) (Shipley Megaposit SPR 700-1.2) film and exposing this film to an interference pattern produced using a 325 nm He–Cd laser. The pattern was chemically developed and then transferred to the silica substrate by reactive-ion etching with a mixture of CHF_3 and O_2 gases. The Alq_3 and silver layers were then in turn deposited on this corrugated substrate.

The third experimental sample (Fig. 2(c)) was constructed in order to examine the emission mediated via SPP modes which were coupled to light from a single scattering surface. The emissive Alq_3 layer differed from that used in the previous samples here being deposited by means of spin coating rather than evaporation. This was achieved by doping a solution of polymethylmethacrylate (PMMA), with Alq_3 (3% by weight) in chloroform. The PMMA/Alq_3 solution was then spin-coated onto the substrate at 4000 rpm the thickness of the resulting film found to be ~160 nm. Subsequently, a silver film of thickness (50 ± 1) nm was thermally evaporated on top of the organic layer. A periodic corrugation was then introduced at the metal/air interface using a focused ion-beam milling system (FEI Nova 600). The corrugation consisted of a grating with square profile having a pitch of 400 nm and a depth of 15 nm; the grating area covered a total of $95\mu m \times 190\ \mu m$.

The next structure studied, shown in Fig. 2(d) was used to study index-coupled SPPs. This sample contained a 43 ± 2 nm thick microstructured metal film ($\lambda_g = 338 \pm 1$ nm) constructed in an identical manner to that used in the sample shown in Fig. 2(b). As with the previous sample, the planar substrate was spin-coated with a solution of PMMA and Alq_3 (3% by weight) in chloroform. Again the thickness of this layer was ~160 nm. The refractive index of this spun emissive layer (~1.46) was less than that of the evaporated Alq_3 film (~1.7). The use of this lower refractive index emitted allowed for a greater choice of media that could be added to the metal/air interface so as to couple the SPP modes supported by the metal film together. This coupling of the SPP modes was achieved by building up layers of a dielectric material at the metal–air interface until the effective refractive indices of the two materials bounding the metal were equal. To this end, monolayers of the material, 22-tricsenoic acid (22-tric) were deposited onto the metal film using the Langmuir–Blodgett (LB) technique [29]. This technique allowed nanometer control of the thickness of the dielectric overlayer, and thus great control over the effective refractive index of the upper air half-space. By increasing the thickness of the dielectric film in this way the effective refractive index at the metal/air boundary could be varied from 1.0 (bare metal) to ~1.58 for a semi-infinite dielectric (22-tric) overlayer thickness. This approach allowed the effective refractive indices of the dielectric material (as seen by the SPP modes) bounding the metal film to be matched by the addition to the metal of a dielectric overlayer of an appropriate thickness.

The final structure studied is shown in Fig. 2(e). The structure consisted of a 55 ± 2 nm thick planar silver film bound on one side by a ~160 nm thick spun Alq_3/PMMA layer. This sample was investigated to explore the use of index-coupled SPP modes further. The other side of the Ag was spin-coated with a PR film, into this film a microstructure was introduced (period $\lambda_g = 485$ nm) using the holographic technique detailed above, the thickness of this microstructured PR film was ~100 nm. The microstructured PR film served two purposes. Firstly, the thickness of the PR film was such that it enabled the effective refractive index of this layer to be matched to the index of the emissive layer, so allowing the SPPs to couple across the metal. Secondly, the microstructure at the PR/air interface enabled the SPP modes supported by the structure to be Bragg scattered to light.

4. Results/analysis

4.1. Modes supported by the structure

Before examining the optical emission from the samples shown in Fig. 2 it was first deemed useful to determine the nature of the various optical modes supported by the structures. This was achieved by measuring the transmittance through the structures as a function of both the angle of incidence and wavelength of the light incident upon the sample. From these data an experimentally derived dispersion map was constructed by converting the collected data to transmittance as a function of both angular frequency and in-plane wavevector. Dispersion maps for TM polarised light incident upon the first two the structures (Fig. 2(a) and (b)) are shown in Fig. 3(a) and (b), respectively. From examination of Fig. 3(a) it may be seen that no modes are supported by this planar structure as the light incident upon the sample is unable to couple to any SPP

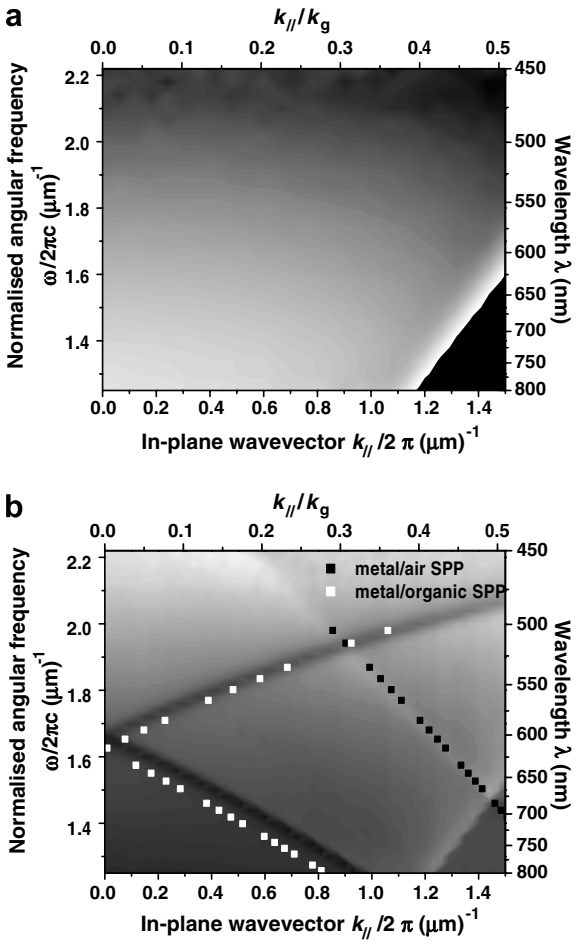

Fig. 3. Dispersion map constructed from experimentally measured transmission data from the experimental samples shown in (a) Fig. 2(a) and (b) Fig. 2(b). Light regions represent high transmission and dark regions represent low transmission. Also shown in (b) is the calculated dispersion of the metal/air (black squares) and metal/organic (white squares) SPPs.

modes due the momentum mismatch mentioned previously. In contrast, from Fig. 3(b) a number of transmission maxima/minima may be seen, these features correspond to incident light coupling to modes supported by the structure. In order to determine the nature of these mode numerical calculations where undertaken.

Using the SPP dispersion relation (Eq. (1)) the in-plane wavevectors of the SPP modes associated with each of the metal interfaces were calculated for a range of angular frequencies (from 1.25 to 2.0 μm^{-1}). The real component of the relative permittivity of silver for each of the values were taken from the literature [30], the relative permittivities of Alq_3 and air were taken to be 2.89 and unity, respectively. By adding/subtracting a grating vector ($\boldsymbol{k}_g$) where appropriate, the in-plane wavevectors of the Bragg-scattered SPPs were calculated. These calculated data are plotted in Fig. 3(b) together with the TM polarised transmittance data. From Fig. 3(b) good agreement may be seen between the calculated SPP in-plane wavevectors and the experimentally measured transmittance data. The transmittance features seen in Fig. 3(b) may therefore be identified as being the result of the TM polarised incident light coupling to SPP modes supported by each of the metal/dielectric interfaces of the structure. (It should be noted that when TE polarised light was incident upon the structure no modes were seen.) Furthermore, as the calculations presented in Fig. 3(b) depend upon the grating vector ($\boldsymbol{k}_g$), this transmission is shown to be result of the SPP modes being Bragg scattering from the microstructured metal film. Note: the discrepancy between the calculated and measured in-plane wavevectors for the metal/organic SPP at lower angular frequencies is due to a single value being used for the relative permittivity of the Alq_3 thus not taking into consideration the dispersion of the refractive index of this layer. Having identified that the samples studied supported SPP modes the structures were further examined in order to see if power coupled to these modes could be recovered as light. To this end PL measurement were taken from each of the structures shown in Fig. 2 and the SPP-mediated emission from each of these samples investigated.

4.2. Photoluminescence measurements

To measure the PL through the silver films each sample was mounted on a rotation stage and the emission measured over a range of polar emission angles θ. The emissive layer was optically pumped through the silica substrate with a 410 nm diode laser, the resulting PL being collected through a small circular aperture that limited the angular acceptance of the emission to approximately 1°. On passing through a polariser, that could be set to pass either TM or TE polarised light, the collected light was focused onto an optical fibre connected to a spectrometer and a charged coupled device (CCD) detector (resolution $\Delta\lambda = 2$ nm). In order to keep the pumping conditions constant the pump angle relative to the sample was maintained constant throughout each experiment.

PL data were measured in the form of emission intensity as a function of both polar emission angle and wavelength, and as with the previous

transmittance data, were converted into the form of a dispersion map. Fig. 4(a) shows the dispersion map constructed from the data measure from the sample shown in Fig. 2(b). The z-axis of this plot represents emission intensity with light regions corresponding to areas of strong emission. From Fig. 4(a) a number of emission maxima may be seen, by comparison with the transmittance data shown in Fig. 3(b) it may be seen that this emission is mediated via the SPP modes previously identified as being associated with each interface of the metal film. These data (Fig. 4(a)) shown that energy lost by excitons within the organic media to SPP modes may be recovered by the introduction into the sample of an appropriate wavelength scale microstructure.

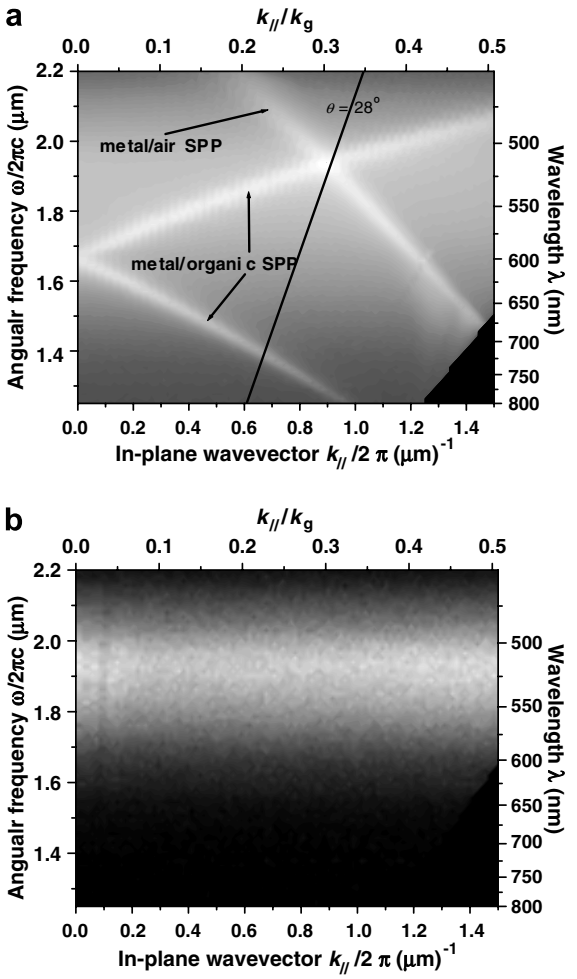

Fig. 4. Dispersion maps constructed from experimentally measured photoluminescence data from the experimental sample shown in (a) Fig. 2(b) and (b) Fig. 2(a). Light regions represent strong emission.

PL measurements were also taken from the planar control sample and these data are shown in Fig. 4(b). From Fig. 4(b) no evidence of PL mediated via SPP modes may be seen. However, the reason for this is not that the structure does not support any SPP modes. In this case the excited emitter may couple to the SPP modes associated with both the metal/organic and metal/air interfaces via the near field [21,31]. The lack of emission from these SPP modes is because the in-plane wavevector of the SPP has no means to match to the in-plane wavevector of photons in air.

To investigate the relative strength of the PL emission from both the metal/organic and metal/air SPP modes individual emission spectra from the samples with planar and microstructured metal films (Fig. 2(a) and (b)) where examined. Fig. 5 shows TM polarised PL spectra measured from the sample with a planar metal film at a polar mission angle of 28° and from microstructured sample at angles of 25°, 28° and 40°. From Fig. 5 a number of features may be seen. For each emission spectrum there is a broad feature with a peak at a wavelength of approximately 520 nm corresponding to the intrinsic emission spectrum of the Alq_3. Additionally for the data collected from the sample with the microstructured metal film a number of sharp emission peaks may be observed. These peaks may be seen to disperse with emission angle, indicative of Bragg scattered modes, they correspond to PL emission mediated via both the metal/organic and metal/air SPP.

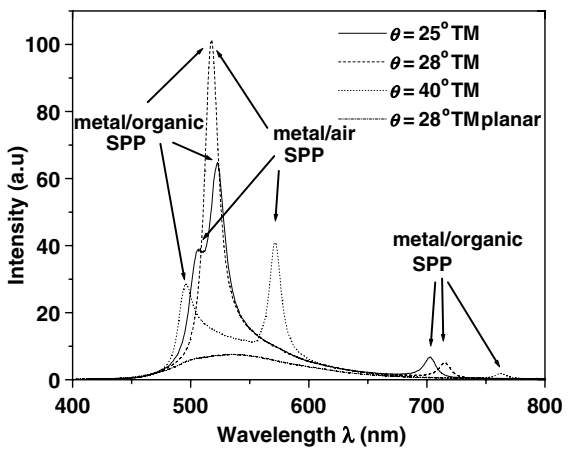

Fig. 5. TM polarised photoluminescence spectra of light emitted from the structure shown in Fig. 2(b) at a polar emission angles θ of 25°, 28° and 40° and from the structure shown in Fig. 2(a) at 28°.

Comparing the SPP-mediated PL from the microstructured sample it can be seen that the relative emission intensities of the metal/organic and metal/air SPPs are approximately equal and seem to depend only upon where the SPP emission peak sits within the Alq_3 intrinsic emission. This appears to be at odds with the data shown in Fig. 1 in which the power coupled to the metal/organic SPP was approximately 100 times greater than the power coupled to the metal/air SPP. To gain an understanding of why this disparity is not seen in the PL emission, the way in which the SPPs may outcouple to light must be considered.

Taking first the SPP mode associated with the metal/organic interface; this mode may couple to light via one of two routes. Firstly, it may be scattered by the microstructure at the metal/organic interface. The light will then be attenuated as it propagates through the metal before emerging into the far-field. Secondly, the microstructure at the metal/air boundary may scatter the mode. In this case it is the attenuated field associated with the metal/organic SPP that is scattered by the microstructure. Emission mediated via either of these two routes is attenuated to a similar degree on crossing the metal film and thus they have a similar amplitude. Recent work [32] has shown that emission via these two out-coupling routes are out of phase with each other, and thus destructively interfere. Therefore, whilst the emitter couples to this mode strongly the resulting emission appears weak.

The emission mediated via the SPP mode associated with the metal/air interface is also attenuated as the power coupled to this mode by the emitter has to cross the metal film. However, this SPP may then scatter from the metal/air interface and emit freely into the far-field. As this emission only occurs by scattering from one interface no cancellation occurs. Thus, whilst this mode is only relatively weakly coupled to by the emitter the intensity of the emission mediated via the metal/air SPP it may be seen to be comparable with that via the metal/organic SPP (Fig. 5).

From the data presented above it may be seen that the introduction into a sample of a wavelength scale microstructure may allow SPP modes to be scattered to light. However, in order to maximize this SPP-mediated emission some means must be sought to overcome the phase cancellation between the two scattering routes open to the metal/organic SPP. One means to achieve this may be to couple the modes associated with the metal/organic and metal/air SPPs together thus allowing energy to be transferred across the metal before being scattered into the far-field. To this end two coupling schemes were considered, grating coupling and index coupling. Also considered was a structure with a thin metal film that was only modulated at one interface. From such a structure SPP modes could only scatter to light from one interface and therefore the phase cancellation route above would be negated.

Fig. 6(a) shows an experimentally derived dispersion map constructed from PL emission measured from the structure shown in Fig. 2(c) [33].

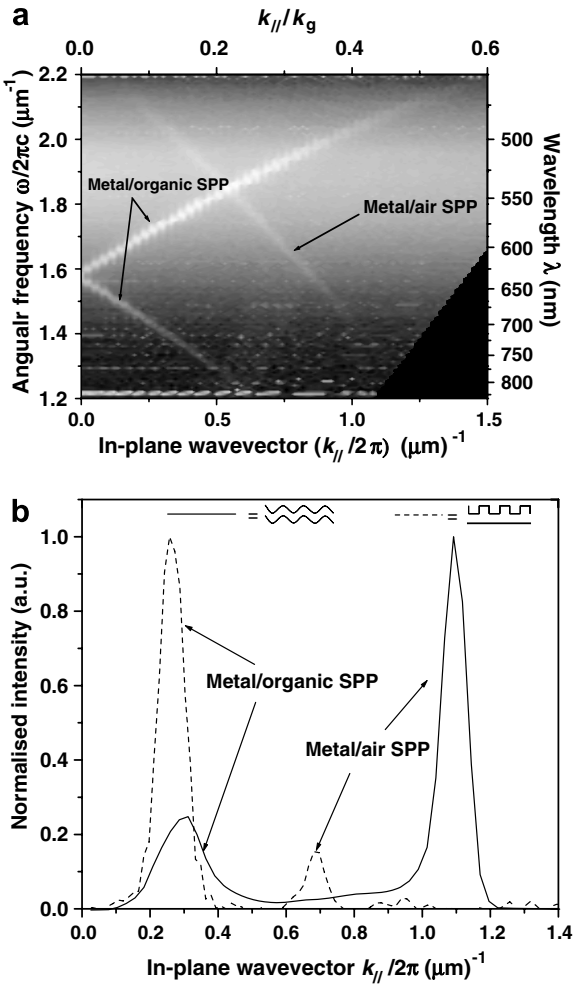

Fig. 6. (a) Dispersion map constructed from TM polarised photoluminescence data from the sample shown in Fig. 2(c) (metal is only textured on top surface the period of grating is 400 nm). (b) Normalised TM polarised photoluminescence intensity measured for two samples shown in Fig. 2(b) (solid line) and (c) (dashed line). Data represented by the solid line were taken at a wavelength of 550 nm, whereas data corresponding to the dashed line were taken at 580 nm.

Comparing these data (Fig. 6(a)) with the corresponding dispersion map constructed from the sample with a symmetrically microstructured metal film (Fig. 4(a)) it may be seen that both plots show evidence of the metal/organic and metal/air SPP modes. There is however one striking difference between the two sets of data, the relative intensity of light mediated via the two SPP modes. From Fig. 4(a) it may be seen that the intensity of the emission mediated by both the metal/organic and metal/air SPPs is very similar in intensity. In contrast the intensity of the emission mediated by the metal/organic SPP is much strong than that emitted by metal/air SPP in Fig. 6(a). This intensity difference is even more evident when the results obtained for the two samples are compared in a single graph, as shown in Fig. 6(b) [33]. These data (Fig. 6(b)) show the normalised PL intensity from each structure plotted as a function of the in-plane wavevector for a given value of angular frequency ($1.82\ \mu m^{-1}$ for the asymmetric structure shown in Fig. 2(c) and $1.72\ \mu m^{-1}$ for the symmetric sample shown in Fig. 2(b)). Fig. 6(b) shows that in the presence of an asymmetric profile of the two interfaces (dashed line) there is a significant increase in PL intensity due to radiative SPPs excited at the metal/organic boundary. These data are consistent with the ideas outlined above, namely that, by removing one of the pathways for emission of the metal/organic SPP, the possibility of destructive interference is removed, resulting in more emission associated with this mode being observed. In turn, this suggests that the efficiency of OLEDs could be increased simply by using a non-conformal geometry for the different metallic interfaces.

The first SPP coupling technique we examined was SPP grating-coupling. From inspection of the PL emission (Fig. 5) from the microstructured sample it may be seen that the maximum emission appears to occur at a wavelength of 518 nm and an emission angle (θ) of 28°. This emission corresponds to the crossing point of the metal/organic and metal/air SPPs and may be seen in Fig. 4(a) at $k_{||} = 0.88\ \mu m^{-1}$ and $\omega = 1.93\ \mu m^{-1}$. Here the wavevectors of the two SPP modes may be matched via scattering from the microstructure satisfying Eq. (3). Energy may therefore be transferred across the metal where it may then scatter to light from the corrugation at the metal/interface (Eq. (2)). However, as this cross-coupled SPP-mediated emission only occurs over a narrow range of emission angles and wavelengths such a scheme may therefore not be best suited to applications such as display devices. Below an alternative SPP coupling scheme is considered.

The second SPP coupling scheme considered was the use of index-coupled SPPs. In this study the SPP modes supported on either side of a metal film were coupled together by the addition to the metal of a dielectric overlayer, see Fig. 2(d). In total nine different dielectric overlayer thicknesses ranging from 26 nm to 198 nm were used with the intensity of the PL emission from the sample measured as a function of dielectric overlayer thickness.

Dispersion maps constructed from the TM polarised PL measured from the samples with dielectric overlayer thicknesses of 46.8 nm, 156.0 nm and 196.8 nm are shown in Fig. 7(a)–(c), respectively [34]. Comparing the position of the SPP mode associated with the metal/air interface from the PL data for the bare microstructured metal sample (Fig. 4(a)) with the same mode for a sample with a dielectric thickness of 46.8 nm (Fig. 7(a)) it may be seen that the addition of the dielectric overlayer causes this mode to shift downwards in frequency. This downshift results from an increase in the wavevector of the SPP mode, given by Eq. (1), associated with the metal/air (now metal/dielectric overlayer-air) boundary as the permittivity at this interface increases with the addition of the dielectric overlayers. This decrease in frequency is seen to continue as the dielectric film thickness is further increased to 156.0 nm (Fig. 7(b)). For dielectric overlayer thicknesses greater than 156.0 nm the position of the metal/dielectric-overlayer/air SPP was seen to remain largely unchanged in frequency (Fig. 7(c)). The observation of two SPP modes with similar frequencies (energies) is consistent with a structure supporting coupled SPP modes and is in agreement with the findings of Gruhlke et al. [27]. In order to determine if the coupling together of the SPP modes supported by the metal film was accompanied by an increase in emission intensity, the PL emission from each of the structures containing a dielectric overlayer was further examined.

For each of the dielectric overlayer thicknesses the PL emission was studied over a range of emission angles (0–40°) and wavelengths (416–806 nm). This was achieved by summing the individual PL spectra obtained at one degree intervals this summed intensity was then plotted as a function of wavelength. The area under each of these curves was then determined by integration to give a mea-

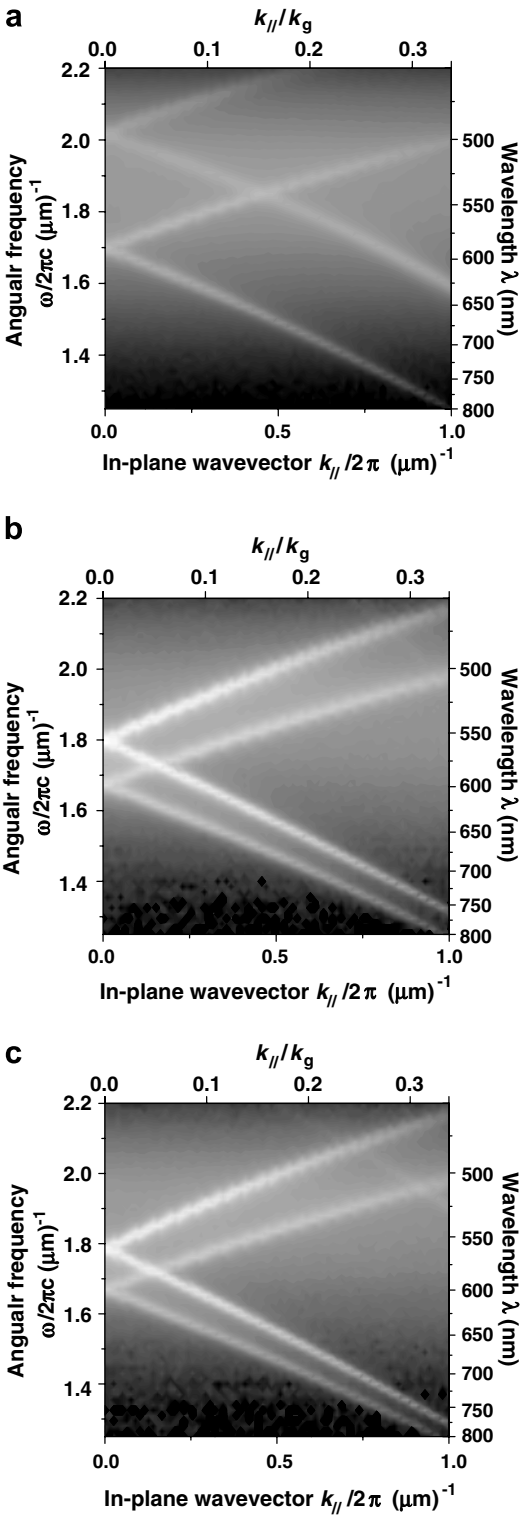

Fig. 7. Dispersion maps showing the TM polarised photoluminescence emission from structures with dielectric overlayer thicknesses of (a) 46.8 nm, (b) 156 nm and (c) 196.8 nm. Light regions indicate areas of strong emission.

sure of the relative emission intensity from each structure.

Fig. 8 shows this integrated emission intensity for both TM and TE polarised emission as a function of dielectric overlayer thickness [34]. Also shown is the integrated TM polarised emission intensity from the planar control sample. From Fig. 8 it may be seen that for dielectric overlayers thicknesses of 26.0–67.6 nm the intensity of the TM polarised PL is the same as that from the microstructured sample with no overlayer, i.e. a bare metal film (to within experimental error). However, as the dielectric overlayer thicknesses further increases the PL emission intensity is seen to increase sharply until a maximum is reached for a dielectric thickness of 156.0 nm. For dielectric overlayer thicknesses greater than ~156.0 nm the emission intensity may be seen to fall. These data (Fig. 8) show the SPP modes are best coupled together for a dielectric overlayer thickness of 156 nm.

For the TE polarised data there were no modes seen for dielectric overlayer thicknesses of less than 114 nm and the data for these samples were approximately equal to the planar structure. For overlayer thickness greater than 114 nm sharp emission features were seen in the PL and corresponded to the recovery of TE polarised waveguided modes associated with the dielectric overlayer. From Fig. 8 it may be seen that for the summed emission associated with the TE polarised emission there was no

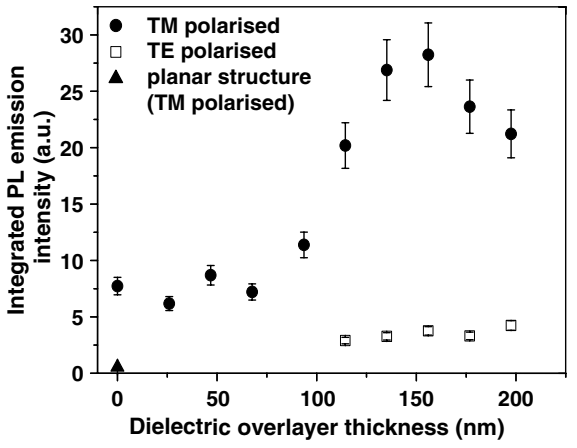

Fig. 8. Integrated intensity of photoluminescence emission as a function of dielectric overlayer thickness from corrugated samples shown in Fig. 2(d). Also shown is the integrated TM polarised photoluminescence emission intensity from a planar control structure (Fig. 2(a)). (Note for dielectric overlayer thicknesses below 114.4 nm no TE polarised emission features were seen.)

increase for dielectric overlayer thicknesses of greater than 114 nm.

The PL data presented in Fig. 8 show that when the SPP modes associated with the metal film are best coupled (dielectric overlayer thickness of 156 nm) the that summed PL emission is ~3 times greater than for a bare microstructure metal film and ~50 times greater than for a planar metal film. However, in term of a commercial device the manufacture of a microstructured metal film may be demanding in terms of fabrication. Below the emission from a device containing a planar metal film which supports coupled SPP and where these modes are scattered to light from a textured dielectric overlayer is examined.

The structure shown in Fig. 2(e) contained a planar metal coated with a microstructured photoresist (PR) film, pitch $\lambda_g = 485 \pm 1$ nm. As noted above this microstructured PR layer served two purposes. Firstly, the thickness of the PR film was such that it enabled the effective refractive index of this layer to be matched to the index of the emissive layer allowing the SPPs to couple across the metal. Secondly, the microstructure at the PR/air interface enabled the SPP modes supported by the structure to be Bragg scattered to light.

Fig. 9 shows the PL emission at an emission angle of 10°, from the samples shown in Fig. 2(a), (b), (d) and (e) labelled planar, grating-coupled, index-coupled and dielectric, respectively [35]. From Fig. 9 it may be seen that the PL from the dielectric and that from the index-coupled samples are comparable. In contrast the PL from the dielectric structure may be seen to be approximately an order of magnitude greater than that from the grating-coupled sample and ~50 times greater than that from the planar structure.

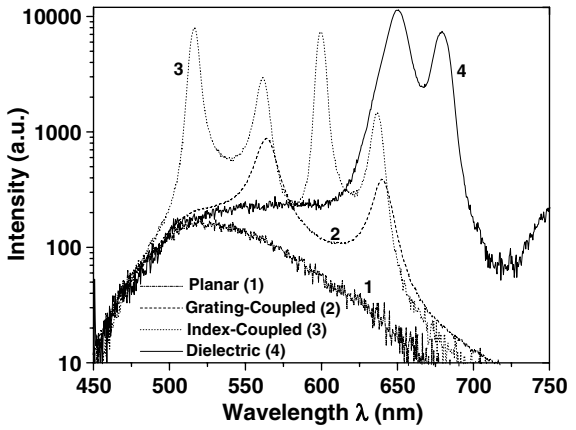

Fig. 9. TM polarised photoluminescence emission spectra measured through the metal film from; planar, grating-coupled, index-coupled and dielectric structures (shown in Fig. 2(a)–(d)), respectively. Each spectrum was measured at a polar emission angle θ of 10°. Note each spectrum has been normalised with respect to the emission spectrum obtained from the planar structure. This normalisation was achieved by fitting the spectra obtained from the three microstructured samples to the spectrum obtain from the planar structure over a wavelength range from 400 nm to 480 nm.

Considering the separation between the Alq_3/PMMA layer and the scattering surface at the PR/air interface (~150 nm) the intensity of the PL from the dielectric structure is remarkable. These data (Fig. 9) illustrate that by introducing an appropriately scaled periodic microstructure into a dielectric film energy lost to SPP modes may be recovered as light.

5. Conclusions

It has been shown that surface plasmon–polariton (SPP) modes supported by a TOLED may provide a significant loss channel thus diminishing the efficiency of the device. The introduction into a structure of an appropriately scale microstructure enables some of this lost power to be recovered as light. However, it has been demonstrated that if this SPP-mediated emission of light is to be optimized careful consideration must be taken over the device geometry. It has been seen that the intensity of light emitted via the SPP mode associated with the metal/organic interface from a metal film that contains a symmetric microstructure is less than might be expected. This is attributed to light mediated via the metal/organic SPP mode that is scattered from the metal/organic interface being in anti-phase with the light mediated from this mode when it is scattered from the metal/air interface and thus leading to cancellation. A thin metal film that incorporates wavelength scale microstructure at a single interface has been used to demonstrate that these phase cancellations may be overcome.

We have also shown that these losses may in part be overcome by selecting a sample geometry that allows the SPP modes associated with either side of a thin metal film to couple, thus enabling energy to be transported across the metal. By the use of grating-coupled and index-coupled SPP modes it has been shown that power might be transported across the metal and that this power may then be scattered to light. However, the emission mediated by grating-coupled SPPs has been seen to occur only

over a narrow range of emission wavelengths and angles and is thus of very limited practical value.

PL emission from a microstructured metal film that supports coupled SPPs has been shown to be ~3 times greater than from a corrugated sample that supports individual SPP modes and ~50 times greater than a similar planar structure. Emission mediated via these index-coupled SPP has been shown to occur across a range of emission angles and wavelengths. We have also shown that similar improvements can be achieved by introducing the microstructure into an overlying dielectric, leaving the metallic cathode planar. This approach should be more compatible with manufacturing processes.

In summary the work presented above has shown that by the careful selection of device geometry power dissipated to otherwise non-radiative SPP modes may be scattered to light. These findings may have the potential to increase the optical efficiency of TOLEDs.

References

[1] J.H. Burroughes, D.D.C. Bradley, A.R. Brown, R.N. Marks, K. Mackay, R.H. Friend, P.L. Burn, A.B. Holmes, Nature 347 (1990) 539.
[2] D. Braun, A.J. Heeger, Appl. Phys. Lett. 58 (1991) 1982.
[3] M.A. Baldo, D. O'Brien, Y. You, A. Shoustiikov, S. Silbey, M.E. Thompson, S. Forrest, Nature 395 (1998) 151.
[4] J.M. Lupton, J. Matterson, I.D.W. Samuel, M.J. Jory, W.L. Barnes, Appl. Phys. Lett. 77 (2000) 3340.
[5] P.A. Hobson, J.A.E. Wasey, I. Sage, W.L. Barnes, IEEE J. Sel. Top. Quantum Electron. 8 (2002) 378.
[6] C.W. Tang, S.A. Van Slyke, Appl. Phys. Lett. 51 (1987) 913.
[7] L.S. Hung, C.W. Tang, M.G. Mason, Appl. Phys. Lett. 70 (1997) 152.
[8] S.A. Van Slyke, C.H. Chen, C.W. Tang, Appl. Phys. Lett. 69 (1996) 2160.
[9] P.A. Hobson, S. Wedge, J.A.E. Wasey, I. Sage, W.L. Barnes, Adv. Mater. 14 (2002) 1393.
[10] V. Buluvic, G. Gu, P.E. Burrows, S.R. Forrest, Nature 380 (1996) 29.
[11] M.-H. Lu, J.C. Sturm, J. Appl. Phys. 91 (2002) 595.
[12] L.S. Hung, C.W. Tang, M.G. Mason, P. Raychaudhuri, J. Madathill, Appl. Phys. Lett. 78 (2000) 544.
[13] S. Han, X. Feng, Z.H. Lu, D. Johnson, R. Wood, Appl. Phys. Lett. 82 (2003) 2715.
[14] M.-H. Lu, M.S. Weaver, T.X. Zhou, M. Rothman, R.C. Kwong, M. Hack, J.J. Brown, Appl. Phys. Lett. 81 (2002) 3921.
[15] Chieh-Wei Chen, Ping-Yuan Hsieh, Huo-Hsien Chiang, Chun-Liang Lin, Han-Ming Wu, Chung-Chih Wu, Appl. Phys. Lett. 83 (2003) 5127.
[16] S.C. Lo, N.A.H. Male, J.P.J. Markham, S.W. Magennis, P.L. Burn, O.V. Salata, I.D.W. Samuel, Adv. Mater. 14 (2002) 975.
[17] T.D. Anthopoulos, M.J. Frampton, E.B. Namdas, P.L. Burn, I.D.W. Samuel, Adv. Mater. 16 (2004) 557.
[18] L.H. Smith, J.A.E. Wasey, W.L. Barnes, Appl. Phys. Lett. 84 (2004) 2986.
[19] H. Raether, Surface Plasmons, Springer-Verlag, Hamberg, 1989.
[20] L.H. Smith, J.A.E. Wasey, I.D.W. Samuel, W.L. Barnes, Adv. Funct. Mater. 15 (2005) 1839.
[21] W.H. Weber, C.F. Eagen, Opt. Lett. 4 (1979) 236.
[22] D. McBranch, I.H. Campbell, D.L. Smith, J.P. Ferraris, Appl. Phys. Lett. 66 (1995) 1175.
[23] R.W. Gruhlke, W.R. Holland, D.G. Hall, Phys. Rev. Lett. 56 (1986) 2838.
[24] R.W. Gruhlke, D.G. Hall, Appl. Phys. Lett. 53 (1988) 1041.
[25] S. Wedge, I.R. Hooper, I. Sage, W.L. Barnes, Phys. Rev. B 69 (2004) 245418.
[26] I. Pockrand, Opt. Commun. 13 (1974) 311.
[27] W. Gruhlke, W.R. Holland, D.G. Hall, Opt. Lett. 12 (1987) 364.
[28] D. Sarid, Phys. Rev. Lett. 47 (1981) 1927.
[29] G.G. Roberts, Langmuir–Blodgett Films, Plenum Press, New York, 1990.
[30] E.D. Palik, Handbook of Optical Constants of Solids, Academic, New York, 1985.
[31] I. Pockrand, A. Brillante, D. Mobius, Chem. Phys. Lett. 69 (1980) 499.
[32] I.R. Hooper, J.R. Sambles, Phys. Rev. B 67 (2003) 235404.
[33] A. Giannattasio, S. Wedge, W.L. Barnes, J. Mod. Opt. 53 (2006) 429.
[34] S. Wedge, S.H. Garrett, I. Sage, W.L. Barnes, J. Mod. Opt. 52 (2005) 833.
[35] S. Wedge, W.L. Barnes, Opt. Exp. 12 (2004) 3673.